

Vortex Analysis in Uncertain Vector Fields

Mathias Otto and Holger Theisel

Otto-von-Guericke University Magdeburg, Germany

Abstract

We present an approach to extract and visualize vortex structures in uncertain vector fields. For this, we generalize the concepts of the most common vortex detectors to uncertain vector fields, namely the λ_2 -criterion, Q -criterion, and the concept of parallel vectors at the example of the method by Sujudi and Haines. All these methods base on the computation of derivatives of the uncertain vector field which are uncertain fields as well. Since they generally cannot be computed in a closed form, we provide a Monte Carlo algorithm to compute the respective probability distributions. Based on this, uncertain versions of vortex regions and core structures are introduced. We present results of our approach on three real world data sets in order to give a proof of concept.

1. Introduction

The analysis of flow fields plays a vital role in many computational fluid dynamics (CFD) applications. As the amount and complexity of CFD data rapidly increases, this raises a need for an efficient and a reliable analysis. Additionally, for many applications not only the amount and complexity is increasing, but also the possibilities *how* data can be acquired and analyzed for one specific case. For instance, because today's computational power, it has become feasible to perform multiple simulation runs with slightly varying parameters resulting in a series of similar vector fields. The same problem holds for experimental data acquisition with measurement errors. This introduces the need to manage and process multiple flow fields describing one and the same phenomenon. Each field has an associated reliability which can be captured by the concept of *uncertainty*. In the certain setting the extraction of flow features is a complex task, but becomes even more challenging for such uncertain flow data. The extraction of specific features such as topology of uncertain vector data has been discussed by Otto et al. [OGHT10] and Schneider et al. [SFRS11]. What is still missing is the treatment of *vortices* in uncertain flow fields.

Following this, we present a method to define a uniform description of common vortex methodologies for uncertain vector fields acquired as a series of flow fields for the same phenomenon. Having this, we can directly compare resulting structures, distributions, and deviations, as well as certainty at which vortex structures are created or appear in specific locations. For our analysis of uncertain fields we will focus on two main directions: the extraction of *vortex cores*

by means of well defined geometric line structures and the definition of *vortex regions* which resemble whole areas of distinct rotational behavior. The main contributions of this paper are:

- We generalize the definition of vortex regions and cores to uncertain vector fields.
- We propose a different model of uncertainty that uses correlations to the probability distributions of the neighborhood. This uncertainty model enables us to compute all vortex extractors by the same Monte Carlo method.
- Finally, we test our method for some real-world data sets and discuss the results.

2. Related work

As mentioned in the previous section, vortex-related features play a central role in the analysis of vector fields. This reflects the amount of literature and approaches existing on this subject. Among CFD applications a set of common standard tools has been settled. Those methods can be grouped into two main categories:

- *Region-based* vortex criteria that define a characteristic scalar field in which closed subsets define distinct regions of vortical behavior. Regarding this, there are the Q -criterion defined by Hunt et al. [HWM88] and the λ_2 criterion by Hussian et al. [JH95]. In addition to this, physically inspired definitions are given by analyzing vorticity magnitude (e.g. described by Zabusky et al. [ZBP*91]), and helicity of the underlying flow field (e.g. as done by Degani et al [DLS90]).

- *Vortex-core-line-based* approaches define binary criteria that describe the location of centers of vortical fluid motion. Such approaches are the Parallel Vectors (PV) operator described by Roth and Peikert [RP98], the Sujudi and Haines vortex core extractor [SH95], and the local pressure minima method by Banks et al. [BS94]. In fact, most of the methods falling into the second category can be generalized by a Parallel Vectors description as shown by Peikert et al. [PR99]. Among those approaches Weinkauff et al. [WSTH07] presented a detector for centers of swirling particle motion, and Sahner et al. [SWH05] a Galilean invariant detection methodology. A scale-space approach is presented by Bauer et al. [BP02].

One subclass of those approaches deals with tracking core line features in order to describe the temporal evolution of vortex structures over time, e.g. Theisel et al. [TSW*05]. As mentioning all existing approaches on this topic is out of the scope of the paper, we refer to the overview about core line based methods is presented by Jiang et al. [JMT04].

However, we focus on uncertain flow data given as a family of similar vector fields. In general the notion of uncertainty has become increasingly popular among many computational applications. The concept of uncertainty itself is already widely spread in the fields of data visualization, (e.g. for the topic of isosurfaces [DKLP02, GR02, RLBS03, Bro04]) and information visualization (e.g. [SPB08]). An approach for scalar fields that is methodically similar to this work is presented in [PWH11]. They extract isosurfaces of uncertain scalar fields by using correlated Gaussian distributions of scalar values. A general overview about uncertain data analysis is presented by Griethe et al. [GS06]. More recently it has been introduced into the field of flow analysis. Here we can identify two subcategories taking different perspectives on the definition of uncertainty:

- *Local* approaches describe uncertainty as a feature that can be evaluated at a point inside the vector field, without considering its long-term integral behavior. Sanderon et al. [SJK04] describe patterns of uncertainty using a reaction-diffusion model, while Botchen et al. [BWE05] introduce a texture-based visualization technique representing local reliabilities by cross advection and error diffusion. The same authors used additional color schemes to emphasize uncertainty [BWE06]. Another approach is presented by Zuk et al. [ZDG*08] using bidirectional vector fields to illustrate the impact of uncertainty.
- In contrast, *global* approaches propagate the information how reliable a certain velocity information is within the flow field. Such global approaches have been presented by Otto et al. for the 2D case [OGHT10], 3D flow fields [OGT11b], and the extraction of special flow features as closed orbits [OGT11a]. In addition to this time-dependent Lagrangian features has been proposed by Schneider et al. [SFRS11] and a glyph-based visualization by Hlawatsch et al. [Hla1].

Considering the mentioned approaches, we already have a set of methods to describe feature extraction in the uncertain setting. However, we are not aware of an adequate approach for vortex detection for such data.

3. Uncertain vector fields

In contrast to certain vector fields an uncertain vector field does have multiple vectors or error measures defined at each point in the spatial domain. This results in a distribution of vectors at each location in an uncertain vector field. In Otto et al. [OGHT10, OGT11b] a definition for a 2D and 3D *uncertain vector field* is given by a $2n$ -dimensional ($n \in \{2, 3\}$) scalar field $\rho(\mathbf{x}; \mathbf{v})$ that describes the transfer from every location $\mathbf{x} \in \mathbf{D}$ to each location $\mathbf{v} \in \mathbb{R}^n$. This field has the following properties:

- $\rho(\mathbf{x}; \mathbf{v}) \geq 0$,
- $\int \rho(\mathbf{x}; \mathbf{v}) d\mathbf{v} = 1$.

where ρ denotes the probability that at the location \mathbf{x} the vector field has some value in the range $\mathbf{v} + d\mathbf{v}$. For a bounded domain the last condition is relaxed such that the integral can be less than or equal to one.

In physics, many phenomena are modeled with Gaussian distributions. Following this, we assume that ρ has the form

$$\begin{aligned} \rho(\mathbf{x}; \mathbf{v}) &= \mathcal{N}(\mathbf{m}(\mathbf{x}), \mathbf{C}(\mathbf{x})) \\ &= \frac{1}{2\pi\sqrt{\det(\mathbf{C})}} e^{-\frac{1}{2}(\mathbf{v}-\mathbf{m})^T \mathbf{C}^{-1}(\mathbf{v}-\mathbf{m})} \end{aligned} \quad (1)$$

where $\mathbf{m} \in \mathbb{R}^n$ is the mean vector field and $\mathbf{C} \in \mathbb{R}^{n \times n}$ is the covariance matrix field.

Technically, our input data are multiple flow data sets over the same regular grid. At the grid point $\mathbf{x}_{i,j}$, we have the m velocity vectors $\mathbf{v}_{i,j,k}$ for $k = 1, \dots, m$ obtained from multiple measurement or simulation. For them we compute the best fitting Gaussian distribution

$$\rho(\mathbf{x}_{i,j}, \mathbf{v}) = \mathcal{N}(\mathbf{m}_{i,j}, \mathbf{C}_{i,j}) \quad (2)$$

where $\mathbf{m}_{i,j} = \frac{1}{m} \sum_{k=1}^m \mathbf{v}_{i,j,k}$ and $\mathbf{C}_{i,j} = \frac{1}{m} \sum_{k=1}^m (\mathbf{v}_{i,j,k} - \mathbf{m}_{i,j})(\mathbf{v}_{i,j,k} - \mathbf{m}_{i,j})^T$. Then (1) is obtained by applying a piecewise bilinear interpolation of $\mathbf{m}_{i,j}$ and $\mathbf{C}_{i,j}$ respectively.

In order to compute vortex structures, the usual way is to compute derived fields from the velocity field which contains its derivatives. In the uncertain case, the derived fields are uncertain fields as well. To compute them, two problems have to be solved:

1. Even if the original field has a Gaussian distribution, the derived fields are not Gaussian. Moreover, the derived fields generally do not have closed form solutions.
2. When computing the uncertain velocity gradient it has to be considered that the distributions at adjacent grid points are correlated.

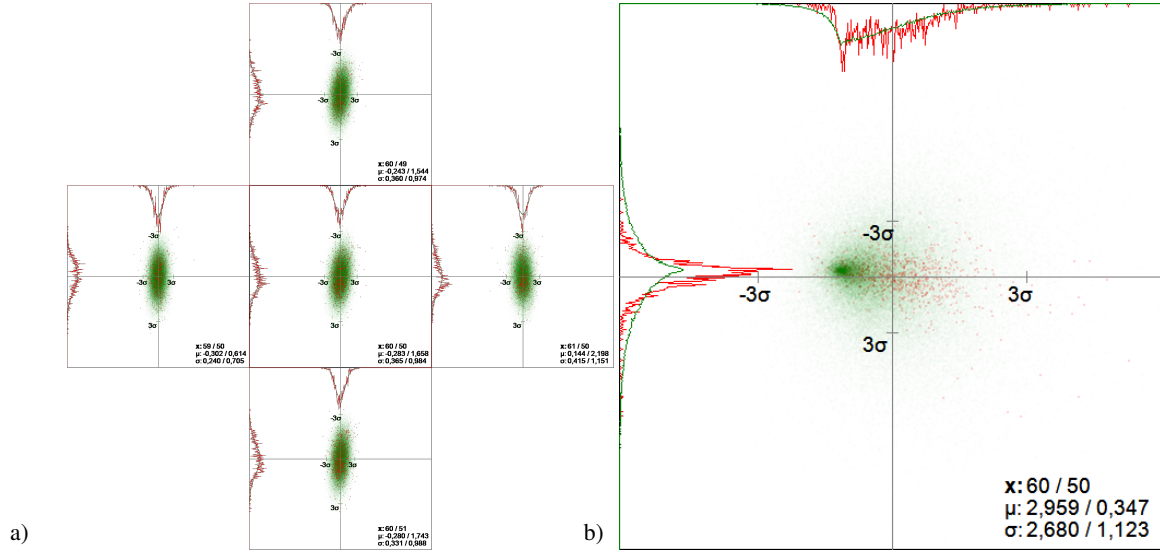


Figure 1: Uncertain velocity and acceleration at grid point (60,50) of the PIV data set using uncorrelated Gaussian distributions. a) sample vectors $\mathbf{v}_{i,j,k}$ as red dots and marginal density distribution as red curves; uncorrelated Gaussian reconstruction and marginal density distribution as green point cloud and curve; b) sampled acceleration and marginal distribution as red point cloud and curves; Monte Carlo sampling of acceleration by using uncorrelated Gaussian at grid points as green point cloud and curves: the red and green curves do not coincide.

We explain and illustrate both problems at an example: the computation of the uncertain acceleration field. In the certain case, acceleration is given as $\mathbf{a} = \mathbf{J}\mathbf{v}$, where \mathbf{J} is the Jacobian matrix. In the uncertain case each component of \mathbf{J} is a 1D probability distribution function for which we assume a Gaussian distribution. However, after the multiplication with the uncertain vector field (which is also a Gaussian distribution), another kind of distribution function results. It is a product distribution which is computable in a closed form for only a few special cases [Cra34]. In fact, only for zero means the product distribution is described by a modified Bessel function of the second kind. In general, the uncertain acceleration cannot be written in a closed form.

To illustrate this, we consider a part of the PIV data set that will be fully introduced later in section 6.3. Here, it is sufficient to mention that at each grid points 1024 velocity vectors were measured, i.e., $m = 1024$, and that we consider the grid point $(i, j) = (60, 50)$. Figure 1a consists of 5 parts. The one in the middle shows the (end points of the) vectors $\mathbf{v}_{i,j,k}$ for $i = 1, \dots, 1024$ as red dots where the median is moved to the image center. This red point cloud already gives an impression of the distribution of $\mathbf{v}_{i,j,k}$. Using a binning technique, the marginal distributions can be shown as red curves on the boundaries of Figure 1a (middle). Note that due to the rather low number of samples, the red curves look non-smooth. Nevertheless, their general shape can be observed. By applying (2) we have computed the Gaussian distribution field at the grid point. We visualize it by a Monte Carlo approach, i.e. by computing a large number (here 100,000) of green random sam-

ple points of the distribution as well as the marginal distributions as green curves. The image clearly shows that a Gaussian distribution is indeed a suitable choice at the considered grid point: the densities of the red and green points are clearly correlated, and the red and green curves are rather similar. The remaining 4 images in Figure 1a show the same for the grid points $(i-1, j)$, $(i+1, j)$, $(i, j-1)$, and $(i, j+1)$ respectively. Figure 1b shows the uncertain acceleration at (i, j) in the following way: for $k = 1, \dots, m$, we compute $\mathbf{a}_{i,j,k} = \mathbf{J}_{i,j,k}\mathbf{v}_{i,j,k}$ where the Jacobian is estimated by central differences $\mathbf{J}_{i,j,k} = \left(\frac{\mathbf{v}_{i+1,j,k} - \mathbf{v}_{i-1,j,k}}{2dx}, \frac{\mathbf{v}_{i,j+1,k} - \mathbf{v}_{i,j-1,k}}{2dy} \right)$ and dx, dy are the grid resolutions. Then $\mathbf{a}_{i,j,k}$ are drawn as red dots in Figure 1b. By binning, the two red curves show the marginal density distributions of $\mathbf{a}_{i,j,k}$. They clearly show that their distributions are *not* Gaussian (problem 1 above). The green point cloud is produced by a Monte Carlo approach in the following way: for $h = 1, \dots, 100000$, we consider random sample vectors $\tilde{\mathbf{v}}_{i,j,h}$, $\tilde{\mathbf{v}}_{i-1,j,h}$, $\tilde{\mathbf{v}}_{i+1,j,h}$, $\tilde{\mathbf{v}}_{i,j-1,h}$, $\tilde{\mathbf{v}}_{i,j+1,h}$ obeying the Gaussian distributions at the respective grid points. From them, we compute the random acceleration vectors as $\tilde{\mathbf{a}}_{i,j,h} = \tilde{\mathbf{J}}_{i,j,h}\tilde{\mathbf{v}}_{i,j,h}$ with $\tilde{\mathbf{J}}_{i,j,k} = \left(\frac{\tilde{\mathbf{v}}_{i+1,j,k} - \tilde{\mathbf{v}}_{i-1,j,k}}{2dx}, \frac{\tilde{\mathbf{v}}_{i,j+1,k} - \tilde{\mathbf{v}}_{i,j-1,k}}{2dy} \right)$. Again, every $\tilde{\mathbf{a}}_{i,j,h}$ is shown as a green dot, and the green curves show the marginal distribution of $\tilde{\mathbf{a}}_{i,j,h}$. The green curves again indicate a non-Gaussian distribution. Moreover, the red and green curves do not coincide, meaning that the chosen model of computing the Jacobian is not appropriate (problem 2).

Our approach to overcome the problems 1 and 2 mentioned above is to use a Monte Carlo approach together with

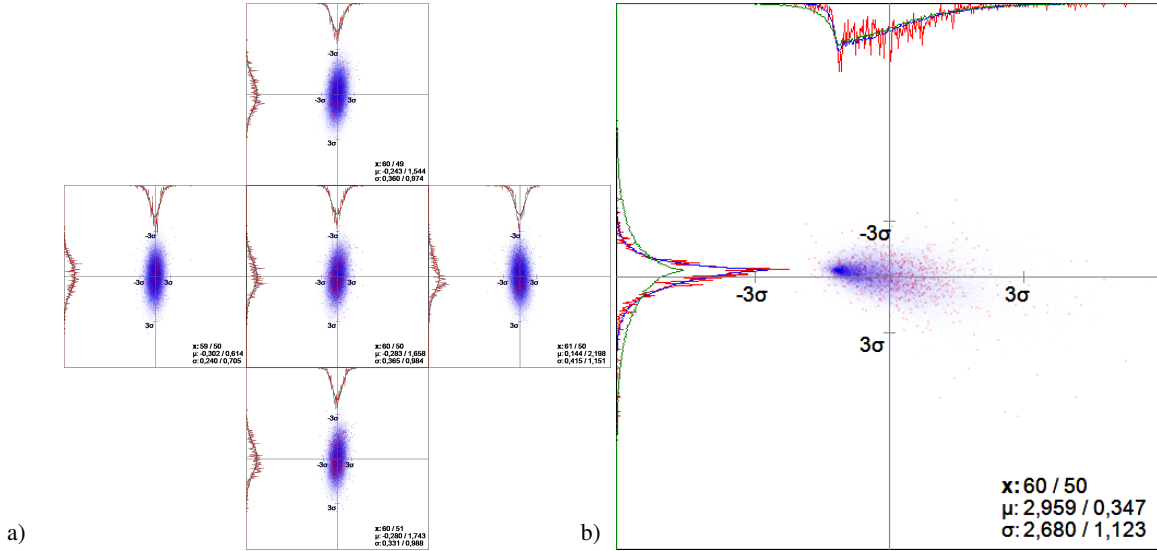


Figure 2: Uncertain velocity and acceleration at grid point (60,50) of the PIV data set using correlated Gaussian distributions. a) sample vectors $\mathbf{v}_{i,j,k}$ as red dots and marginal density distribution as red curves; correlated Gaussian reconstruction and marginal density distribution as blue point cloud and curve; b) sampled acceleration and marginal distribution as red point cloud and curves; Monte Carlo sampling of acceleration by using correlated Gaussian at grid points as blue point cloud and curves: the red and blue curves coincide.

a correlated estimation of the Jacobian. Monte Carlo methods [KW86] are a standard approach to solve probabilistic problems. For considering the correlation between adjacent grid points, we do a simultaneous Gaussian fitting at a grid point and its neighbors. Instead of considering the n -dimensional vectors $\mathbf{v}_{i,j,k}$, we consider the $5n$ -dimensional vectors $\bar{\mathbf{v}}_{i,j,k} = (\mathbf{v}_{i,j,k}, \mathbf{v}_{i-1,j,k}, \mathbf{v}_{i+1,j,k}, \mathbf{v}_{i,j-1,k}, \mathbf{v}_{i,j+1,k})^T$ for $k = 1, \dots, m$. For them, we apply a $5n$ -dimensional Gaussian fitting

$$\rho(\mathbf{x}_{i,j}, \bar{\mathbf{v}}) = \mathcal{N}(\bar{\mathbf{m}}_{i,j}, \bar{\mathbf{C}}_{i,j}) \quad (3)$$

where $\bar{\mathbf{m}}_{i,j}$ is the $5n$ -dimensional median and $\bar{\mathbf{C}}_{i,j}$ is the $5n \times 5n$ covariance matrix. Note that (3) contains both the distributions of the velocity and Jacobian at (i, j) .

Figure 2 illustrates the application of (3) to the same example as in Figure 1. Figure 2a shows the vectors $\bar{\mathbf{v}}_{i,j,k}$ as points distributed over the 5 adjacent grid points; the red curves denote the marginal distributions. The Gaussian distribution is computed by (3) and is shown by the blue point cloud and the blue curves. The coincidence of the red and blue curves show the correctness of the assumption of Gaussian distribution of $\bar{\mathbf{v}}_{i,j,k}$. Figure 2b shows the uncertain acceleration. The red point clouds and curves are identical to Figure 1b. The blue point clouds and curves show the distribution of the acceleration by using (3). Here we can clearly see the coincidence of the red and blue curves, which means that our correlated Gaussian model correctly reproduces the uncertain acceleration (the green curves show the result of the uncorrelated distribution from Figure 1b for comparison.)

So far, we have an approach which can correctly deal with uncertain derived fields containing only the velocity and the Jacobian. Fortunately, many common vortex concepts fall into this category. We are now ready to discuss them in detail.

4. Vortex detection in uncertain vector fields

At first, we want to define a vortex in an uncertain vector field. Even in the certain case several definitions exist. In general, it is described by a swirling motion of a fluid around a core line [RC91, Por97]. In the uncertain case such a well defined core line does not exist. Here we have to deal with density distribution functions that express the movement of particles inside the flow. For the movement of such particle density functions we can only compute probabilities that particles of this distribution move around a core line. The core line itself is not a distinct line structure. We can compute such a line only for one sample of the uncertain vector field. The overall result is a probability for the existence of a vortex core in a small region.

Now we consider the results of vortex detectors. There are two categories: line-based and region-based vortex criteria. In the certain case vortex core line detectors generate a binary decision whether there is a core line at a certain location or not. Vortex region extractors compute scalar fields that describe the strength of the vortical motion. Level sets on this fields are defined representing vortical structures. For the computation of vortical structures in uncertain vector fields the types of resulting fields change. Computing vortex

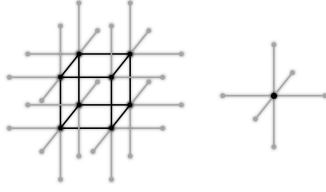


Figure 3: (left) Scheme of the support regions for discrete vortex core line computations in 3D space. The cell we want to evaluate is colored black. (right) Scheme of the support region of vortex region.

cores of such fields results in a probability for the occurrence of a vortical motion at a given location. For uncertain vortex region detectors the result is a 1D density distribution function describing the probabilities of values representing the strength of vortical motion at every location.

We will adapt Q and λ_2 criteria as examples for vortex regions and the method proposed by Sujudi and Haines using the Parallel Vectors operator, as an examples for vortex cores detectors, to uncertain vector fields.

4.1. Vortex cores

One famous method to compute vortex core lines is the Parallel Vectors operator [RP98]. The general approach is to find two derived vector fields of the vector field \mathbf{v} that are parallel where a vortex core line exists. The Parallel Vectors operator is able to express a lot of vortex core line criteria [PR99]. We will consider the method proposed by Sujudi and Haines [SH95]. This method searches points of zero curvature. It can be computed by using the Parallel Vectors operator of the vector field \mathbf{v} and its acceleration field \mathbf{a} , because zero curvature exists where the acceleration field is parallel to the original vector field $\mathbf{a} \parallel \mathbf{v}$.

We will apply this to Parallel Vectors operator to uncertain vector fields. For this we have to compute the probability that two uncertain vectors are parallel. A second condition of the Parallel Vectors operator is that vortex cores only exist where the Jacobian of the vector field has two imaginary Eigenvalues. In section 3 we have shown that this is not possible in a closed form. Therefore, we use a Monte Carlo method that calculates the probability of a vortex core line in a cell of a uniform data grid. The support region for discrete vortex core line computation is shown in Figure 3 (left). It contains 32 data points. Thus, every data point of the uncertain vector field consists of a 96D mean vector and a 96×96 dimensional covariance matrix. We generate N samples of the uncertain vector field. From these sample vectors we compute the acceleration vectors \mathbf{a}_s at the cell nodes. Vortex core lines do not consist of isolated points where the vectors of both fields are parallel, they are continuous lines that cross cells. So we need to compute parallel vectors on the boundary of

each cell. As described by Roth and Peikert [RP98], we assume linear interpolation on all triangles of the cell boundary to get an analytic solution for the parallel vectors computation on the boundary. The probability for the occurrence of a vortex core line inside the cell is the relative frequency of the sampled Parallel Vectors operator on its boundary faces. It is given by:

$$P_{SH} = \frac{1}{N} \sum_{s=1}^N \begin{cases} 1 & \text{if } \mathbf{a}_s \parallel \mathbf{v}_s \wedge \#(\lambda_{im}(\mathbf{J}_s)) = 2 \\ 0 & \text{otherwise} \end{cases} \quad (4)$$

with N as the number of samples. At least two faces have to contain a vortex core that the cell is marked. The high-dimensional Gaussian distribution described by equation (3) is used to generate samples of the uncertain vector field including \mathbf{v}_s . Using these samples \mathbf{J}_s and \mathbf{a}_s are computed.

4.2. Vortex regions

Two of the most common vortex region detectors are the λ_2 criterion [JH95] and the Q criterion [HWM88]. Both criteria make use of the decomposition of the Jacobian \mathbf{J} in a symmetric part $\mathbf{S} = \frac{1}{2}(\mathbf{J} + \mathbf{J}^T)$ and an antisymmetric part $\mathbf{\Omega} = \frac{1}{2}(\mathbf{J} - \mathbf{J}^T)$. The λ_2 criterion is defined by the second largest Eigenvalue of the matrix $\mathbf{S}^2 + \mathbf{\Omega}^2$ and the Q criterion by $\frac{1}{2}(\|\mathbf{S}\|^2 + \|\mathbf{\Omega}\|^2)$.

To apply these criteria to uncertain vector fields we use a Monte Carlo method that samples the uncertain vector field, computes for each sample the Jacobian and the respective criteria. In this case, we need a support region containing the six direct neighbors of the node we want to evaluate and the node itself (Figure 3(right)). Therefore, the uncertain vector field is defined by 21D mean vectors and 21×21 covariance matrices. This results in a 1D histogram of the distribution of the criteria for each data point. The challenge is the visualization. In the certain case vortical structures are enclosed by level sets of the criteria. For the uncertain case we search for a similar visualization. We can visualize the probability that the Q criterion is larger and the λ_2 criterion is smaller than a certain threshold:

$$P(Q > t) = \frac{1}{N} \sum_{s=1}^N \begin{cases} 1 & \text{if } Q_s > t \\ 0 & \text{otherwise} \end{cases} \quad (5)$$

$$P(\lambda_2 < t) = \frac{1}{N} \sum_{s=1}^N \begin{cases} 1 & \text{if } \lambda_{2s} < t \\ 0 & \text{otherwise} \end{cases} \quad (6)$$

with N as number of samples generated from the Gaussian function described in equation (3), Q_s and λ_{2s} are the vortex criteria based on these samples. The visualization shows the probability that at a location with a probability $P > 0$ is enclosed by a level set. If there is no uncertainty, our method returns the same results as the approaches for vector fields without uncertainty.

5. Implementation

We implemented our uncertain vortex framework in C# using the Task Parallel Library for parallelization. The input of our method is a number of vector fields (measured or simulated) describing the same flow phenomenon. These vector fields are given on uniform grids. Using only one vector field corresponds to the certain case. The results of our methods are scalar fields that represent probabilities of vortex criteria. All computations are done on a small local region and are repeated multiple times. This makes our method easy to parallelize using parallel for-loops.

For each local operation a support region is defined. For these regions we generate multivariate Gaussian distributions of the input vectors. These distribution functions represent the uncertain vector field. Samples of such distribution functions are created by a pseudo random generator. A uniformly distributed vector is generated (same dimension as the mean vector of the Gaussian of the support region). To this vector we apply a Box Muller filter that transforms it into a Gaussian distribution. After that, we multiply it with the Eigenvector matrix of the covariance matrix (Eigenvectors are scaled by their Eigenvalues) and add the mean vector. Finally, we split the large vector into 3D vectors according to the nodes of the support region.

With this sample vector set we can compute all vortex criteria. We repeat the sampling and the vortex criteria computation a few hundred times. For region-based vortex criteria we count the number of sample sets with a vortex criterion larger or smaller than a given threshold. Concerning vortex core lines we count the number of sample sets for which the Parallel Vectors operator returns true. The final result is the relative frequency of the positive events.

6. Results

To test our approach we apply our methods to two real-world examples, a flow around a cylinder and a flow field from a climate simulation. All results are generated with a laptop containing an Intel i7 2820QM with 4 cores and HT and 16GB RAM. All data sets were provided by domain experts, who gave positive feedback on the results.

6.1. Flow around a cylinder

In this example we have got four simulations of a flow around a cylinder with different Reynolds-numbers. The Reynolds numbers are between 290 and 320 based on the free stream velocity and the diameter of the cylinder. The flow should be laminar at these Reynolds numbers, but should already show three-dimensional structures. Therefore, only three-dimensional configurations are retained. The time-dependent computations have been performed for 100 seconds physical time. Every 50th time step (every second physical time) is stored for further analysis. The numerical

computations have been performed using the open-source software package OpenFOAM 1.6 using finite volume discretization. Block-structured grids are applied using 645,120 hexahedral elements refined at the cylinder wall. A constant inlet velocity boundary condition is considered at the inlet, pressure outlet at the outlet and symmetry conditions are chosen for the top, bottom and side boundaries. No-slip boundary condition is employed on the cylinder wall. The size of the domain is selected at least 20 times the cylinder diameter to eliminate the reflection on the boundaries.

We resampled the data set to a uniform grid of the domain $[-1, 11] \times [-3, 3] \times [-3, 3]$ with a resolution of $200 \times 100 \times 100$. Then we applied our techniques to this data set. As a helpful orientation all of our result images show LIC of the corresponding mean field in the background. At first we started with the region-based techniques illustrated in Figure 4. Here, from left to right the time steps 98 to 100 are shown. The first row gives an overview of the uncertainty in the data set. In the second row we illustrate the results of our uncertain λ_2 vortex detector. These images show iso-surfaces for $P(\lambda_2 < -0.003) = 0.05$ and 0.95 . The next two rows show analog results of the uncertain Q criterion for $P(Q > 0.003)$. Similar to the certain setting probabilities for Q and λ_2 level sets are correlated. Also regions of strong uncertainty correlate with these level sets. Results of the Parallel Vectors operator are shown in Figure 5 for the same time steps. In the volume renderings and cross-sections we see the probabilities for the occurrence of vortex cores. The extracted volumes where the probability for vortex cores is larger than zero are much smaller than the volumes extracted by the region-based methods. High probabilities only appear at the vortex cores behind the cylinder. The rest of the extracted structures has a rather small probability, but larger volumes.

For time step 100 we make a more detailed analysis. We show a comparison of the λ_2 and Q criteria to the input fields (shown as colored isolines) and the mean field (black isolines) in Figure 6. Regions with high probability correspond to the average level sets and regions with lower probability capture almost all regions of the level sets of the input fields. In Figure 7 we compare our vortex core extractor with the vortex cores of the input fields and the mean vector field. Here, also the level set with 10% probability corresponds to the vortex cores of the mean vector field, and the cores of the input fields are almost captured by regions with less probability. The overall computation time for λ_2 , Q and vortex cores is 3 hour and 40 minutes for each time step, using 200 samples for each data point.

6.2. Ocean ensemble simulation

The ocean simulation data is part of the CMIP5 runs (Coupled Model Intercomparison Project). The model itself is the MPI-OM ocean model which was developed by the Max-Planck Institute for Meteorology in Hamburg. The simula-

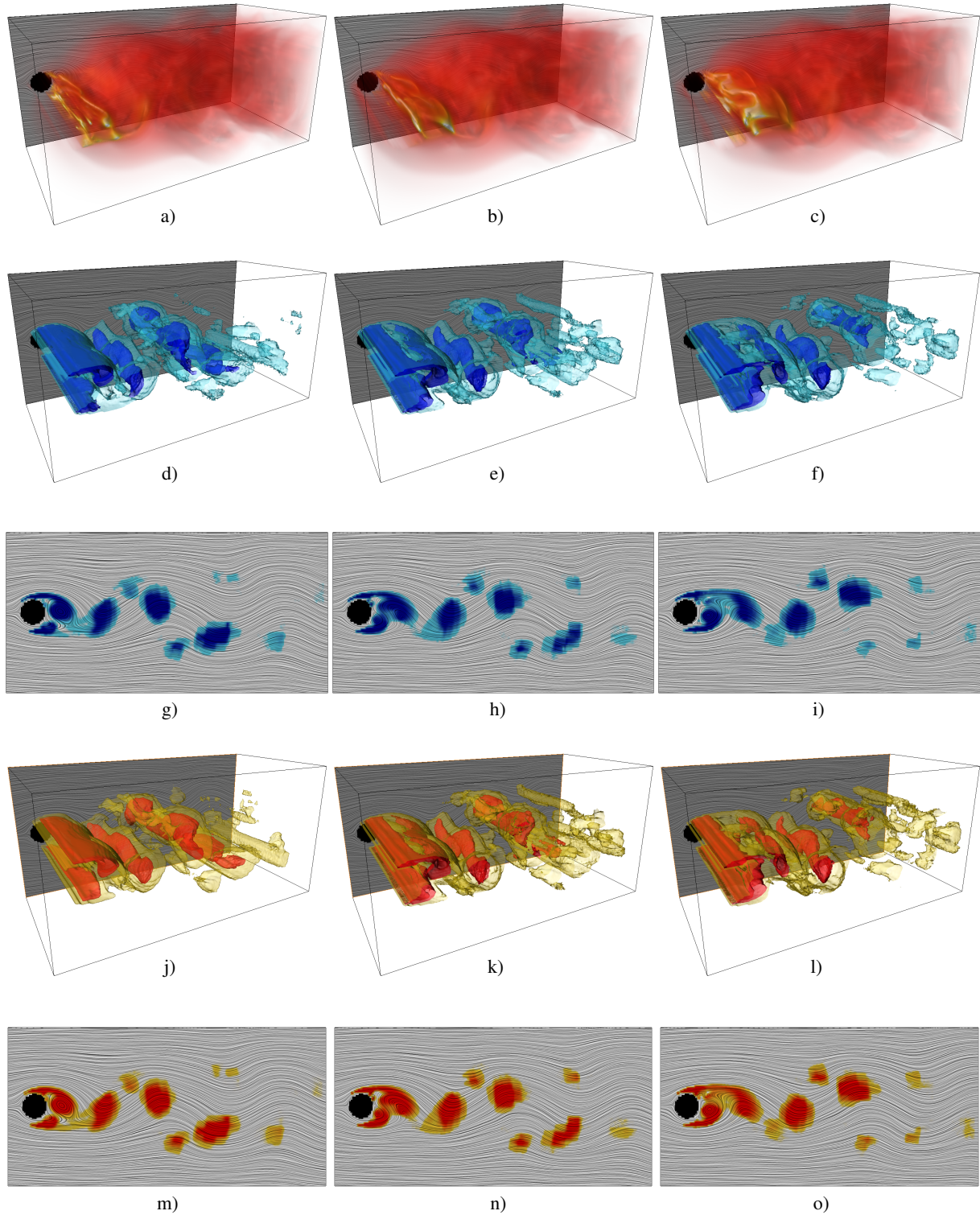


Figure 4: Cylinder data set: **(a,d,g,j,m)** time step 98, **(b,e,h,k,n)** time step 99, **(c,f,i,l,o)** time step 100, **(a,b,c)** volume rendering of the maximal standard deviation, **(d,e,f)** isosurfaces of the probability field $P(\lambda_2 < -0.003)$ with iso values 0.05 and 0.95, **(g,h,i)** cross section of the probability field $P(\lambda_2 < -0.003)$ at $z = 0$ **(j,k,l)** isosurfaces of the probability field $P(Q > 0.003)$ with iso values 0.05 and 0.95, **(m,n,o)** cross section of the probability field $P(Q > 0.003)$ at $z = 0$.

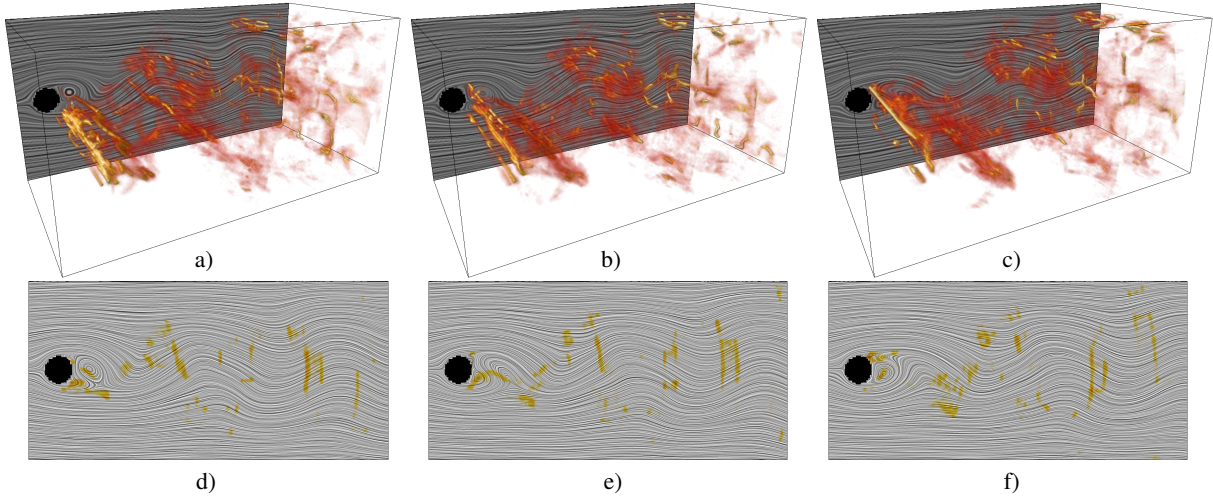


Figure 5: Cylinder data set: (a,d) time step 98, (b,e) time step 99, (c,f) time step 100, (a,b,c) volume rendering of the of the vortex core probability field, (d,e,f) cross section of this field at $z = 0$.

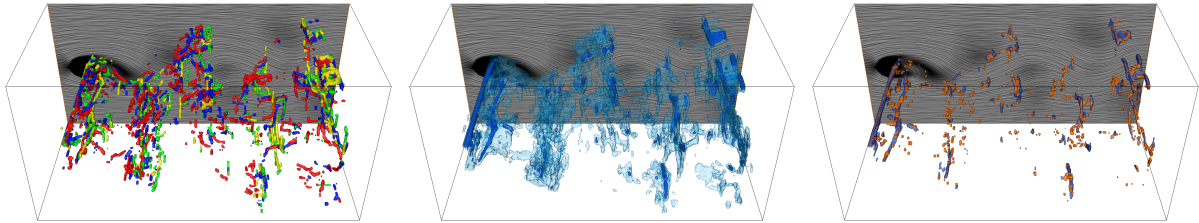


Figure 7: Cylinder data set time step 100: (left) vortex cores of the input vector fields, (middle) isosurfaces of $P(\mathbf{a}_p \parallel \rho) \geq 0.01$ (light blue) and 0.1 (blue), (right) isosurface 0.1 (blue) with vortex cores of the mean vector field (orange).

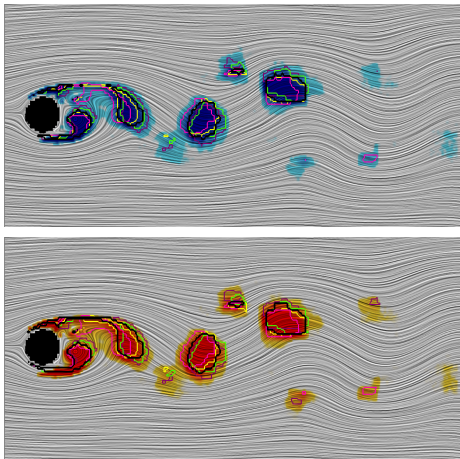


Figure 6: Cylinder data set time step 100: (top) cross section of the probability field $P(\lambda_2 < -0.003)$ and (bottom) $P(Q > 0.003)$ at $z = 0$ compared with isolines of the input data.

tion was carried out on a tri-polar curvilinear grid with a horizontal resolution of 1.5 degree at 40 height levels. Prior to the analysis, the data was resampled to a rectilinear grid. The data set consists of just three scalar variables (uko, vke, wo) that describe the ocean currents. The simulation was performed using an ensemble run, and all together, 10 ensembles with the monthly mean of the currents were used.

Clearly visible in all results (see Figure 8) is the Antarctic circumpolar current, as well as the equatorial currents in the Pacific ocean and the gulf stream and the north Atlantic current in the Atlantic ocean. Especially the circumpolar current which is rich on vortices is detected very well using all criteria. With a higher resolution simulation, probably also smaller features, such as the Kuroshio in Japan, and the Agulhas current at the south-eastern tip of Africa can be detected. The overall computation time for this data set is 1 hour and 16 minutes using 200 samples per grid point.

6.3. Measured PIV data set

Here, we have got 1024 measurements of a flow around a backward-facing step using particle image velocimetry

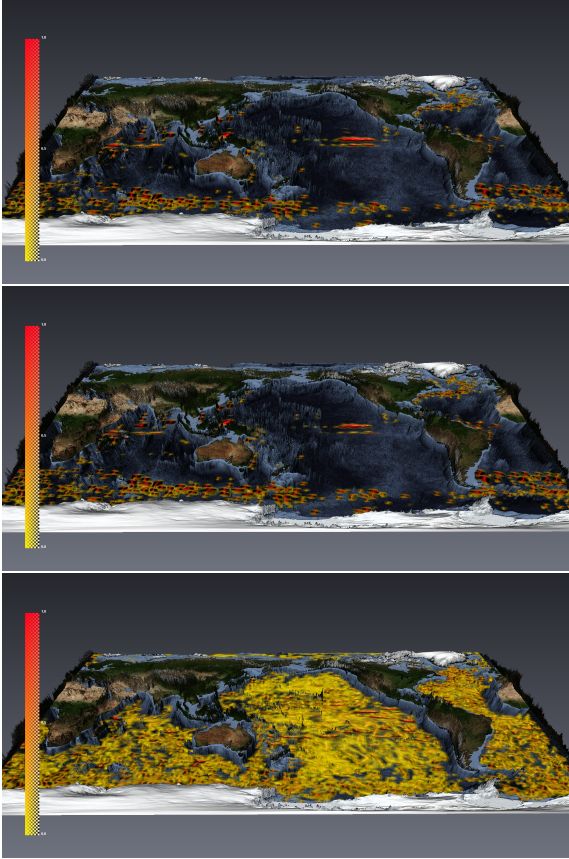


Figure 8: CMIP5 data set: (*top*) showing $P(\lambda_2 < -0.003)$, (*middle*) $P(Q > 0.003)$, and (*bottom*) the probability of vortex cores.

(PIV). From the measurements 1024 2D vector fields were reconstructed which are the input of our methods. All vector fields have the dimension 105×103 . Figures 9a and b shows two examples of the input vector fields.

We applied the region-based vortex criteria to this data set. Figure 9c illustrates the probability that the Q criterion has a larger isovalue than zero, while Figure 9d shows the probability of the λ_2 criterion for isovalues smaller than zero. For comparison Figure 9e shows the Q criterion and Figure 9d the λ_2 criterion of the mean vector field. The probability fields contain only values less than 100%. Also, the results of the mean vector fields do not always correlate with the probability fields. That means there are some configurations that locally differ completely from the average field. For example, the λ_2 criterion of the mean field has some large positive values above the step, while the probability computed by our method shows clearly that there are values smaller than zero. The overall computation time for this data set was 8 minutes and 20 seconds. We used 10,000 samples for each data point.

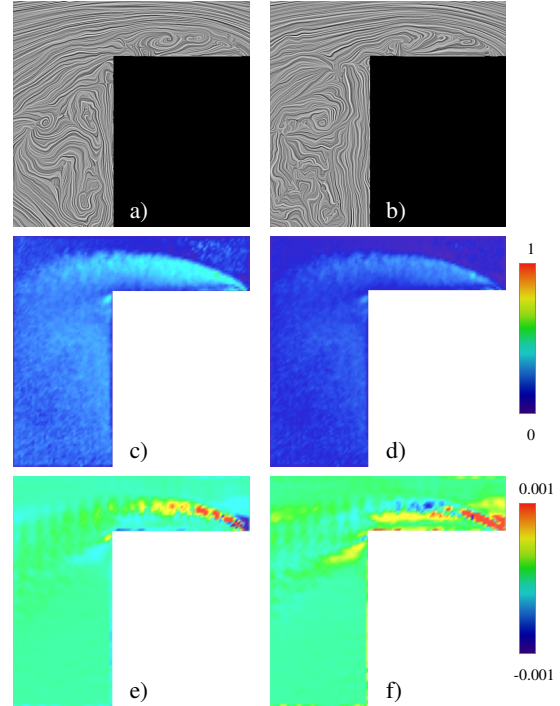


Figure 9: Flow around a backward facing step: (a) and (b) are two examples of reconstructed vector fields of the PIV measurements; (c) $P(Q > 0)$, (d) $P(\lambda_2 < 0)$, (e) Q criterion of the mean vector field, (f) λ_2 criterion of the mean vector field.

7. Conclusion and future work

To the best of our knowledge, we presented the first approach that considers vortex structures of uncertain vector fields. We generalized the concepts of the λ_2 criterion, the Q criterion, and the Parallel Vectors operator at the examples of the method proposed by Sujudi and Haimes to vector fields with uncertainty. For this, we introduced an uncertainty model that incorporates local correlation between vector data of neighboring discrete data points, instead of a purely local vector density distribution function.

In the future we plan to implement our techniques using the GPU to increase the performance. This is not straight forward, because a lot of input fields have to be managed in the memory of the GPU. Finding other uncertainty models that have correlated distribution functions in the support region is another future challenge. We also want to extend our approach to more vortex criteria and other grid types.

Acknowledgments

We thank Gabor Janiga (University of Magdeburg) for the cylinder data set, Niklas Röber (DKRZ) for the ocean data set, and J. Boree and L. Brizzi (Lab. d'Etudes Aérodynamiques de Poitiers) for the PIV data set. This work was funded by the Sem-Seg project under the EU FET-Open grant 226042.

References

- [BP02] BAUER D., PEIKERT R.: Vortex tracking in scale-space. In *Proceedings of the symposium on Data Visualisation 2002* (Aire-la-Ville, Switzerland, Switzerland, 2002), VISSYM '02, Eurographics Association, pp. 233–ff. 2
- [Bro04] BROWN R.: Animated visual vibrations as an uncertainty visualisation technique. In *GRAPHITE* (2004), pp. 84–89. 2
- [BS94] BANKS D. C., SINGER B. A.: Vortex tubes in turbulent flows: identification, representation, reconstruction. In *IEEE Visualization* (1994), pp. 132–139. 2
- [BWE05] BOTCHEN R. P., WEISKOPF D., ERTL T.: Texture-based visualization of uncertainty in flow fields. In *IEEE Visualization* (2005), pp. 647–654. 2
- [BWE06] BOTCHEN R. P., WEISKOPF D., ERTL T.: Interactive visualization of uncertainty in flow fields using texture-based techniques. In *Intl. Symp. on Flow Visualization* (2006). 2
- [Cra34] CRAIG C. C.: On the frequency function of xy . *Ann. Math. Statist.* 7, 1 (1934), 1–15. 3
- [DKLP02] DJURCILOV S., KIM K., LERMUSIAUX P. F. J., PANG A.: Visualizing scalar volumetric data with uncertainty. *Computers and Graphics* 26, 2 (2002), 239–248. 2
- [DLS90] DEGANI D., LEVY Y., SEGNER A.: Graphical visualization of vortical flows by means of helicity. *AIAA Journal* 28 (1990), 1347–1352. 1
- [GR02] GRIGORYAN G., RHEINGANS P.: Probabilistic surfaces: point based primitives to show surface uncertainty. In *IEEE Visualization* (2002), pp. 147–154. 2
- [GS06] GRIETHE H., SCHUMANN H.: The visualization of uncertain data: Methods and problems. In *SimVis* (2006), pp. 143–156. 2
- [Hla1] HLAWATSCH, MARCEL AND LEUBE, PHILIPP AND NOWAK, WOLFGANG AND WEISKOPF, DANIEL : Flow Radar Glyphs - Static Visualization of Unsteady Flow with Uncertainty . *IEEE TVCG* 17, 12 (2011), inprint. 2
- [HWM88] HUNT J. C. R., WAY A., MOIN P.: *Eddies, stream, and convergence zones in turbulent flows*. Center for Turbulence Research Report CTR-S88, Stanford University, 1988. 1, 5
- [JH95] JEONG J., HUSSAIN F.: On the identification of a vortex. *Journal of Fluid Mechanics* 285, -1 (1995), 69–94. 1, 5
- [JMT04] JIANG M., MACHIRAJU R., THOMPSON D.: Detection and visualization of vortices. *Visualization Handbook* (2004), 287–301. 2
- [KW86] KALOS M. H., WHITLOCK P. A.: *Monte Carlo methods. Vol. 1: basics*. Wiley-Interscience, New York, NY, USA, 1986. 4
- [OGHT10] OTTO M., GERMER T., HEGE H.-C., THEISEL H.: Uncertain 2D vector field topology. *CGF (Proc. Eurographics)* 29, 2 (2010), 347–356. 1, 2
- [OGT11a] OTTO M., GERMER T., THEISEL H.: Closed stream lines in uncertain vector fields. In *SCCG* (2011). 2
- [OGT11b] OTTO M., GERMER T., THEISEL H.: Uncertain topology of 3d vector fields. In *Proceedings of 4th IEEE Pacific Visualization Symposium (PacificVis 2011)* (Hong Kong, China, March 2011), pp. 67–74. 2
- [Por97] PORTELA L.: *On the Identification and Classification of Vortices*. Phd thesis, Stanford University, School of Mechanical Engineering, 1997. 4
- [PR99] PEIKERT R., ROTH M.: The "parallel vectors" operator - a vector field visualization primitive. In *IEEE Visualization* (1999), pp. 263–270. 2, 5
- [PWH11] PÖTHKOW K., WEBER B., HEGE H.-C.: Probabilistic marching cubes. *CGF* 30, 3 (2011), 931 – 940. 2
- [RC91] ROBINSON S. K., CENTER. A. R.: *The kinematics of turbulent boundary layer structure*. National Aeronautics and Space Administration, Ames Research Center, 1991. 4
- [RLBS03] RHODES P. J., LARAMEE R. S., BERGERON R. D., SPARR T. M.: Uncertainty visualization methods in isosurface rendering. In *Eurographics* (2003), pp. 83–88. 2
- [RP98] ROTH M., PEIKERT R.: A higher-order method for finding vortex core lines. In *IEEE Visualization* (1998), pp. 143–150. 2, 5
- [SFRS11] SCHNEIDER D., FUHRMANN J., REICH W., SCHEUERMANN G.: A variance based file like method for unsteady uncertain vector fields. In *TopoInVis* (2011). 1, 2
- [SH95] SUJUDI D., HAIMES R.: Identification of swirling flow in 3-d vector fields. *Journal of Fluid Mechanics* 285 (1995), 69–94. 2, 5
- [SJK04] SANDERSON A. R., JOHNSON C. R., KIRBY R. M.: Display of vector fields using a reaction-diffusion model. In *IEEE Visualization* (2004), pp. 115–122. 2
- [SPB08] STREIT A., PHAM B., BROWN R.: A spreadsheet approach to facilitate visualization of uncertainty in information. *IEEE TVCG* 14, 1 (2008), 61–72. 2
- [SWH05] SAHNER J., WEINKAUF T., HEGE H.-C.: Galilean invariant extraction and iconic representation of vortex core lines. In *EuroVis* (2005), pp. 151–160. 2
- [TSW*05] THEISEL H., SAHNER J., WEINKAUF T., HEGE H.-C., SEIDEL H.-P.: Extraction of parallel vector surfaces in 3d time-dependent fields and applications to vortex core line tracking. In *IEEE Visualization* (2005). 2
- [WSTH07] WEINKAUF T., SAHNER J., THEISEL H., HEGE H.-C.: Cores of swirling particle motion in unsteady flows. *IEEE TVCG (Proc. IEEE Visualization)* 13, 6 (28. October - 1. November 2007), 1759–1766. 2
- [ZBP*91] ZABUSKY N. J., BORATAV O. N., PELZ R. B., GAO M., SILVER D., COOPER S. P.: Emergence of coherent patterns of vortex stretching during reconnection: A scattering paradigm. *Phys. Rev. Lett.* 67 (Oct 1991), 2469–2472. 1
- [ZDG*08] ZUK T., DOWNTON J., GRAY D., CARPENDALE S., LIANG J.: Exploration of uncertainty in bidirectional vector fields. In *Society of Photo-Optical Instrumentation Engineers (SPIE) Conference Series* (2008), vol. 6809, p. 68090B. 2